Structure of molten iron chloride: Neutron scattering and modeling

David L. Price, Marie-Louise Saboungi, and Yaspal S. Badyal
Argonne National Laboratory, Argonne, Illinois 60439

John Wang and Simon C. Moss
University of Houston, Houston, Texas 77204

Robert L. Leheny
University of Chicago, Chicago, Illinois 60637

(Received 1 October 1997)

Neutron-diffraction measurements of molten $FeCl_3$, combined with model calculations and computer simulations, show that on melting the local structure of Fe changes from an octahedral to a tetrahedral environment. A similar change is observed in $AlCl_3$, in contrast to YCl_3, for example, where the octahedral coordination of Y is preserved on melting. The local structure of the liquid can be described in terms of Fe_2Cl_6 molecular units, similar to those observed in the vapor phase but with strong intermolecular interactions. Detailed information about the orientational correlations between molecules is derived from the simulations and compared with recent results on another molecular liquid, propylene glycol. [S0163-1829(98)05417-4]

I. INTRODUCTION

Iron trichloride shares with aluminum chloride the distinction of being a trivalent metal halide salt exhibiting an anomalously high increase of entropy and molar volume on melting.[1] Such halides crystallize into a variety of structures, generally characterized by close-packed layers of the halide ions with the metal ions occupying an appropriate fraction of interstitial sites between these layers.[2] These sites can have either octahedral or tetrahedral coordination: for example, in $AlCl_3$ nearly hexagonal Cl layers are stacked in an fcc sequence and the Al ions lie in octahedral sites between two oppositely directed Cl_3 triangles, while in $AlBr_3$ nearly hexagonal Br layers are in an hcp sequence, the Al ions lie in tetrahedral sites on bilayers above and below the Br layers, and two adjacent Al ions together with six Br ions on adjacent layers form Al_2Br_6 molecules.[3] Similar structural differences occur in the melts.[1] Diffraction studies[4] and model calculations[5] of molten YCl_3 show that it has a close-packed structure, similar to that of the crystal but with some disordering of the Cl ions, while molten $AlBr_3$ and $GaCl_3$ are tetrahedrally coordinated with M_2X_6 molecules surviving into the liquid phase.[6] The most interesting situation occurs when the compound undergoes a structural change on melting from octahedral to tetrahedral coordination, which appears to be the case for both $AlCl_3$ (Ref. 7) and $FeCl_3$.[8] The different behavior in melting can be inferred from the large range of values for the change in entropy ΔS and in specific volume $\Delta V/V$, shown for some trivalent metal chlorides in Table I. For example, $FeCl_3$, with $\Delta S=17.8$ e.u. and $\Delta V/V=0.63$, contrasts dramatically with YCl_3 with $\Delta S=7.6$ e.u. and $\Delta V/V=0.005$.

Our previous neutron-diffraction study of $FeCl_3$ (Ref. 8) indicated tetrahedral coordination for the Fe ions and suggested the presence of Fe_2Cl_6 molecular units similar to those observed in the vapor phase.[9] Similar results were obtained in high-energy x-ray-diffraction measurements.[10] Our studies of graphite intercalated with $FeCl_3$ showed an analogous behavior: the intercalated layers form a two-dimensional liquid of Fe_2Cl_6 molecules at high temperature,[11] while at lower temperatures[12] they form a close-packed hexagonal arrangement similar to the bulk crystal.[13] On the other hand, the evidence from Raman scattering[14–16] is less clear: there are strong indications of tetrahedral bonding, but the peak frequencies are quite different from those observed for Fe_2Cl_6 in the vapor phase[17] and calculated for Fe_2Cl_6 molecules on the basis of *ab initio* molecular orbital theory.[18] Further, the value of the ionic conductivity is much higher than that of other trivalent salts where M_2X_6 molecules have been identified (Table I). In this paper we report the results and analysis of a neutron-diffraction measurement on bulk liquid $FeCl_3$, combined with model calculations and molecular-dynamics (MD) simulations, to address the issues of the Fe ion coordination and the existence of Fe_2Cl_6 molecular units in the melt.

II. NEUTRON-DIFFRACTION EXPERIMENT

$FeCl_3$ material, 99.999% purity, obtained from APL Engineering Materials Inc., was encapsulated in vitreous silica

TABLE I. Physical properties of some trivalent metal chlorides (Ref. 5).

Salt	T_m (K)	ΔS_m (c.u.)	$\Delta V/V$[a]	σ (Ω^{-1} cm^{-1})
$InCl_3$	859		0.61	0.42
$AlCl_3$	466	18.1	0.88	5×10^{-7}
$GaCl_3$	351	7.4	0.17	2×10^{-6}
$BiCl_3$	505	5.0	0.22	0.38
$SbCl_3$	347	8.7	0.17	2×10^{-4}
YCl_3	994	7.6	0.005	0.39
$FeCl_3$	577	17.8	0.63	0.04[b]

[a]Relative difference of specific volume of liquid at T_m and that of solid at room temperature.
[b]Reference 15.

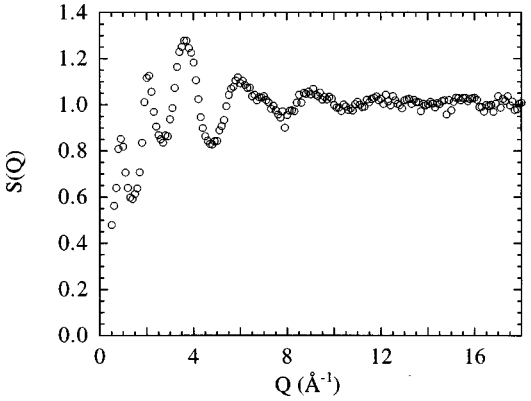

FIG. 1. Measured structure factor of molten $FeCl_3$ at 320 °C.

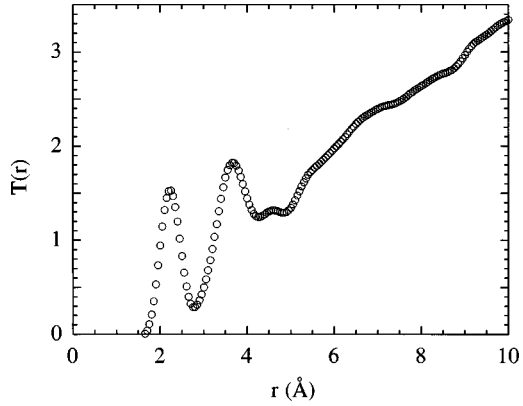

FIG. 2. Pair-correlation function of molten $FeCl_3$ at 320 °C.

tubes 4 mm I.D., 5 mm O.D., 100 mm high with a loading sufficient to fill the beam height of 50 mm when molten. Neutron-diffraction measurements were carried out at the GLAD facility at the Intense Pulsed Neutron Source. The sample was heated to 325 °C in a vacuum furnace inside a cylindrical vanadium element. The structure factor $S(Q)$ was obtained after correcting the measured diffraction patterns for multiple scattering, absorption, and inelastic effects using standard procedures. For the present sample, it was necessary also to subtract the paramagnetic scattering from the Fe. This was calculated on the basis of magnetic moment of 3.2 μ_B (Ref. 10) and the published free-ion form factor.[19]

The corrected neutron average structure factor $S(Q)$ is shown in Fig. 1. This represents a weighted average of the Faber-Ziman partial structure factors $S_{ab}(Q)$:

$$S(Q)=\frac{1}{\langle\overline{b}\rangle^2}\sum_{ab} c_a c_b \overline{b}_a \overline{b}_b S_{ab}(Q), \qquad (1)$$

where c_a and $\overline{b}_a$ are the concentration and coherent neutron scattering length of element a and $\langle\cdots\rangle$ represents an average over the system. $S(Q)$ exhibits a three-peak structure with peaks at wave vector $Q=0.9$, 2.05, and 3.65 Å^{-1}, respectively. Scaling with the nearest-neighbor distance $r_1 \approx 2.22$ Å (see below) gives $Qr_1 \approx 2.0$, 4.6, and 8.1, respectively, typical of values found for the first sharp diffraction peak (FSDP), the Coulomb peak and the topological ordering peak, respectively, in complex liquids.[20] A similar three-peak structure was observed in the x-ray-diffraction pattern of $FeCl_3$ intercalated in graphite at 350 °C.[11]

The neutron average pair-correlation function

$$T(r)=4\pi\rho r+\frac{2}{\pi}\int_0^{Q_{\max}} Q[S(Q)-1]\sin(Qr)dQ, \qquad (2)$$

where ρ is the total number density, is shown in Fig. 2. It has a well-defined first peak which can be fitted by a Gaussian function centered at 2.22 Å. Converting $T(r)$ to the radial distribution function $n(r)$ gives an average coordination number of 3.8 about each Fe, indicating a predominately tetrahedral coordination: the octahedral coordination found in the crystalline phase is clearly ruled out. There is some possibility of dissociation in molten $FeCl_3$, leading to $FeCl_2$ and free Cl_2;[9] however, in the present experiment, since $S(Q)$ is normalized to 1.0 at high Q, values of the coordination number about the Fe ions would be 33% higher than those observed, so this is also inconsistent with the data. The second peak in $T(r)$ is a broad peak centered at about 3.7 Å with a coordination number of 6–7, again considerably lower than the mean value in the crystal, 9.25.

Electron-diffraction data on the Fe_2Cl_6 molecule in the vapor can be fitted by either a planar (D_{2h}) or puckered (C_{2v}) bitetrahedron.[9] In either case the distances of the Fe atoms to the terminal and bridging Cl atoms are 2.13 and 2.33 Å, respectively; the average, 2.23 Å, is in good agreement with the present result. The second-neighbor correlations, predominantly Cl-Cl, give an average distance of 3.59 Å for both D_{2h} and C_{2v} configurations and a coordination number of 3. The present results clearly indicate a very similar short-range order in the liquid. However, in the results from the MD simulations discussed in Sec. IV, based on Fe_2Cl_6 molecules, intermolecular correlations contribute about the same as intra-ones to the second peak of $T(r)$ and in fact extend beyond them on both the low-r and high-r side. Thus, while a description in terms of Fe_2Cl_6 molecules may be appropriate, these molecules are strongly packed and spatially correlated with each other so that a given Cl ion will interact as strongly with its second-neighbor Cl ions on adjacent molecules as with those on the same molecule. We return to this point in Sec. V. In this context, it should be noted that the x-ray-diffraction pattern for $FeCl_3$ intercalated in graphite at 350 °C (Ref. 11), was fitted satisfactorily by a liquidlike layer of Fe_2Cl_6 molecules tilted so as to present Cl_3 triangles to the graphite planes above and below. The present results are very consistent with those of our previous neutron-diffraction experiment[8] and with a recent measurement with high-energy x rays.[10]

III. MODEL CALCULATIONS

In order to derive detailed information about the structure of the melt, several model calculations of $S(Q)$ and $T(r)$ were performed to compare with the experimental data. First, the random packing of structural units (RPSU) model[21,22] was used, due to its inherent simplicity. In this model the neutron average structure factor is given by

$$S(Q)=f_1(Q)+f_2(Q)[S_c(Q)-1]-\frac{\langle\overline{b^2}\rangle}{\langle\overline{b}\rangle^2}+1, \qquad (3)$$

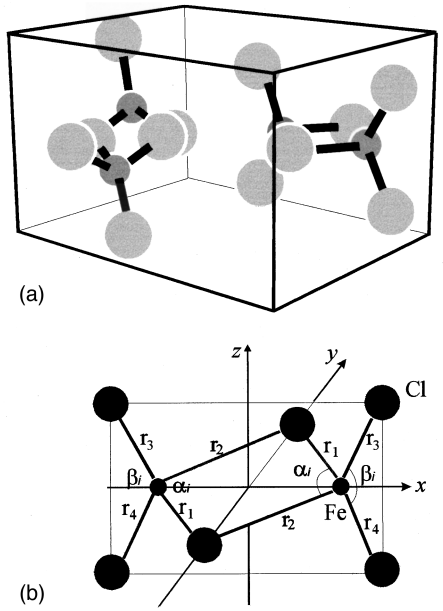

FIG. 3. (a) Schematic representation of two $FeCl_3$ molecules in the models described in Sec. III; (b) definition of internal molecular parameters for Fe_2Cl_6.

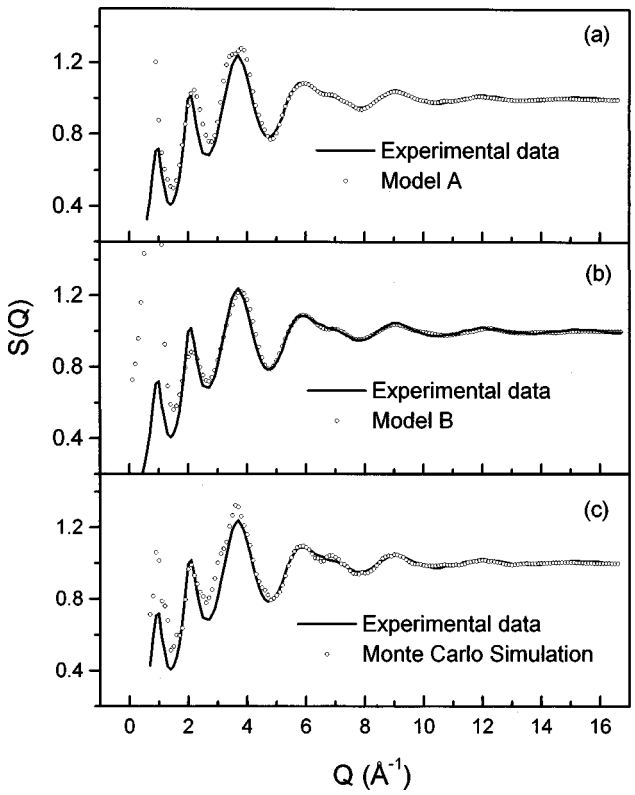

FIG. 4. Comparison of experimental structure factor with those derived from the models described in Sec. III.

where $f_1(Q)$ is the form factor of the isolated molecule, $f_2(Q)$ is a different form factor expressing the average orientational correlation between a pair of molecules, and $S_c(Q)$ is the structure factor for the molecular centers. Initially, $f_1(Q)$ was calculated from the Fe_2Cl_6 vapor phase molecular structure[9] and $S_c(Q)$ from the Percus-Yevick solution of the hard-sphere model with appropriate values for the hard-sphere diameter and packing fraction; $f_2(Q)$ was calculated in two different ways, (a) assuming uncorrelated orientations, and (b) incorporating orientational correlations with the procedures developed by Egelstaff, Page, and Powles.[21] No satisfactory agreement could be obtained in either case, especially with respect to the FSDP and the second peak in $T(r)$, even after refining the molecular structure and hard-sphere parameters.

In the second step, the structural unit in the RPSU model was taken as a pair of Fe_2Cl_6 molecules [Fig. 3(a)] arranged as in the crystal structure of $AlBr_3$ which, as discussed above, retains an Al_2Br_6 molecular structure in the crystal.[6] The internal structures of the two Fe_2Cl_6 molecules were refined. The values of the intramolecular parameters, defined in Fig. 3(b), for the optimized fit (Model *A*) are given in Table II, and the results for $S(Q)$ and $T(r)$ are compared with the data in Figs. 4(a) and 5(a), respectively. Keeping the internal bond lengths fixed, the relative positions (x_c, y_c, z_c) and orientations (α, β, γ) of the two molecules as well as the internal bond angles (α_i, β_i) within the molecules were then refined. The resulting parameters for the new optimized fit (Model *B*) are given in Table II, and the results are displayed in Figs. 4(b) and 5(b). It is seen that the FSDP remains greatly exaggerated in both models (a consequence of having purely hard-sphere packing of the two-molecule structural units), but the subsequent peaks in $S(Q)$, and both main peaks in $T(r)$, are rather well fitted, especially for Model *B*.

In the final step, the optimized pair of Fe_2Cl_6 molecules obtained in Model *B* were placed in the unit cell of a 54-molecule nanocrystal with the Al_2Br_6 structure.[3] The internal molecular structure was then refined with a Monte Carlo

TABLE II. Molecular structure parameters for Models *A* and *B* (Sec. III).

	r_1 (Å)	r_2 (Å)	r_3 (Å)	r_4 (Å)	α_i (°)	β_i (°)	x_c[a]	y_c[a]	z_c[a]	α (°)[b]	β (°)[b]	γ (°)[b]
						Model *A*						
Molecule 1	2.345	2.192	2.21	2.213	96.17	104.15	[c]	[c]	[c]	[c]	[c]	[c]
Molecule 2	2.233	2.143	2.261	2.261	108.80	95.70						
						Model *B*						
Molecule 1	2.1	2.1	2.25	2.25	105.99	63.53	0.792	0.667	0.747	47.46	−7.45	8.18
Molecule 2	2.1	2.1	2.25	2.25	108.59	112.83						

[a]Given as fractions of the unit-cell parameters.

[b]α, β, and γ are rotations about the z, x, and y axes, respectively.

[c]As in the $AlBr_3$ crystal.

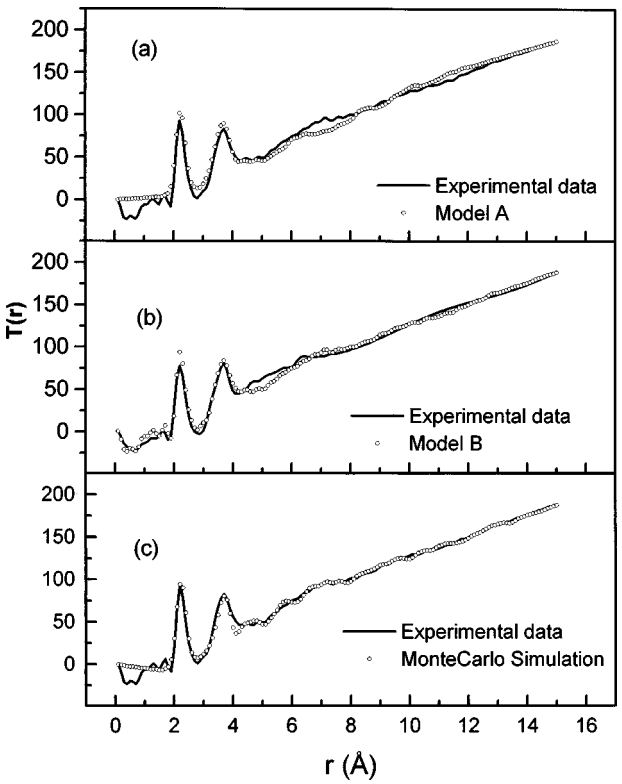

FIG. 5. Comparison of experimental pair-correlation function with those derived from the models described in Sec. III.

technique. Although the resulting $S(Q)$ and $T(r)$ were naturally more strongly peaked than the data, the overall agreement in terms of peak positions and intensities was encouraging. The intermolecular positions and orientations were then refined, again with a Monte Carlo technique, keeping the internal structure fixed. The resulting fits, after 1000 Monte Carlo steps, are displayed in Figs. 4(c) and 5(c). The agreement of the model $S(Q)$ with the data is reasonably good—the second (Coulomb) peak is reproduced but the FSDP and third peaks, associated with topological ordering, are still too high—and the fit for $T(r)$ is excellent.

Overall, one can conclude from these calculations that (a) a model based on Fe_2Cl_6 molecules, distorted somewhat from their structure in the vapor, is able to reproduce the experimental data for the liquid, except for the FSDP, and (b) the $AlBr_3$ crystal structure, which retains the Al_2Br_6 unit in the crystal, provides a good starting point for the arrangement of these molecules. This structure must reflect to some degree the close packing and spatial correlations between molecules in the $FeCl_3$, $AlCl_3$, and $AlBr_3$ melts.

IV. MOLECULAR-DYNAMICS SIMULATIONS

The model calculations described in the previous section made no assumptions about the nature of the bonding. As an alternative approach, a molecular-dynamics simulation was carried out, based on close-packed Fe_2Cl_6 molecules and using parametrized forms for the interatomic potentials in the literature. The simulation consisted of 150 Fe_2Cl_6 molecules at 320 °C and used Biosym/MSI's Discover 3 software using the extensible systematic force field,[23] which contains potentials for each atom that include bond length, bond angle,

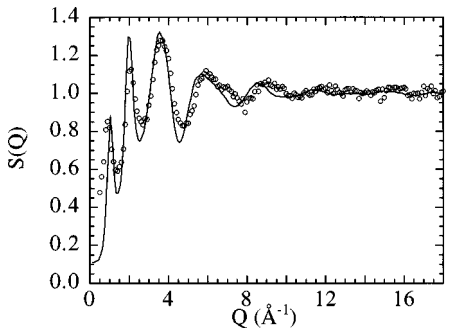

FIG. 6. Comparison of experimental structure factor (circles) with that derived from the simulation described in Sec. IV (line).

torsional, and out-of-plane interactions in the molecules as well as van der Waals and Coulombic interactions between nonbonding atoms. The simulation lasted 500 ps with a time step of one fs. The molecules were constrained in a cell with periodic boundary conditions and with a volume set by the experimental density. (The resulting pressure in the simulated liquid was approximately 3300 atmospheres.) The position of each atom was recorded every 5 ps, for a total of 100 configurations, to obtain adequate statistics for calculating structure factors and pair-correlation functions. Figure 6 compares the neutron structure factor $S(Q)$ calculated from the simulation with that obtained experimentally. The simulation reproduces each feature in the measured structure factor, lending further support to the conclusion that $FeCl_3$ is a molecular liquid almost fully comprised of Fe_2Cl_6 molecules.

The three partial structure factors $S_{ab}(Q)$, $(a,b)=(\mathrm{Fe,Cl})$, obtained from the simulation are displayed in Fig. 7. The FSDP at $Q \approx 1.0$ Å^{-1} results primarily from the first peak in $S_{\mathrm{FeFe}}(Q)$, with a smaller contribution arising from $S_{\mathrm{ClFe}}(Q)$. The origin of the FSDP is often described[22] in terms of scattering from correlated structural units, in this case Fe_2Cl_6 molecules. Because of the Fe atoms' central positions in each molecule, interference between scattering from Fe in different molecules strongly reflects the topologi-

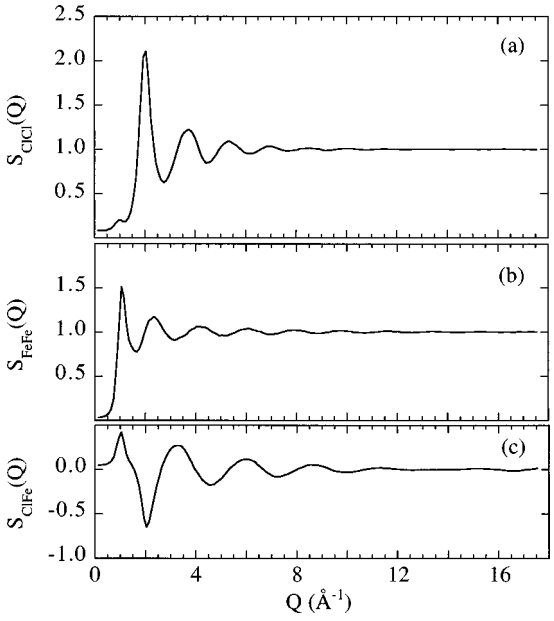

FIG. 7. Partial structure factors derived from the simulation.

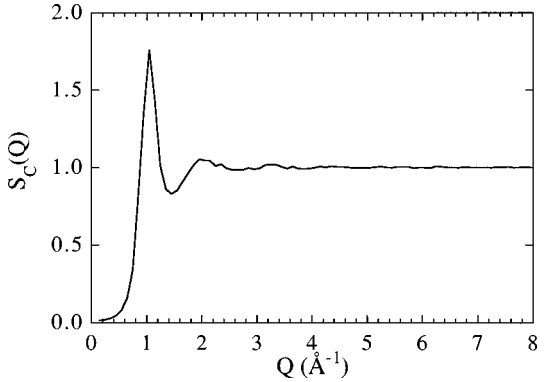

FIG. 8. Structure factor for the molecular centers derived from the simulation.

cal ordering of the molecules, giving rise to this peak. Direct calculation of the structure factor for the molecular centers, $S_c(Q)$, shown in Fig. 8, reveals a first peak at the same position as the FSDP, confirming this interpretation. The second peak in $S(Q)$ results primarily from the first peak in $S_{\mathrm{ClCl}}(Q)$ and is attenuated by a large negative peak in $S_{\mathrm{ClFe}}(Q)$. A similar cancellation by different partial structure factors occurs in molten AB salts between $S_{AA}(Q)$ and $S_{AB}(Q)$.[1] In these systems this effect results from charge transfer between the species that leads to a preference for unlike species as nearest neighbors. In the case of $FeCl_3$, since much of the contribution to this peak comes from intermolecular scattering, the relative orientations of neighboring molecules augment the molecular structure in leading to this effect. The third peak in $S(Q)$ derives primarily from a peak in $S_{\mathrm{ClFe}}(Q)$ and can be associated with the topological ordering given by the well defined Fe-Cl bond length. This feature in $S(Q)$ and all features at higher Q result primarily from intramolecular scattering. Figure 9, which displays the intramolecular contribution to the structure factor, $S_{\mathrm{intra}}(Q)$, demonstrates the close match between $S_{\mathrm{intra}}(Q)$ and $S(Q)$ above $Q \approx 4$ Å^{-1}.

As Fig. 6 reveals, the peak positions from the simulation's $S(Q)$ become increasingly shifted from the measured peaks in the region where intramolecular scattering dominates. This disagreement indicates that the bond lengths in the simulated molecules do not exactly match those in the real

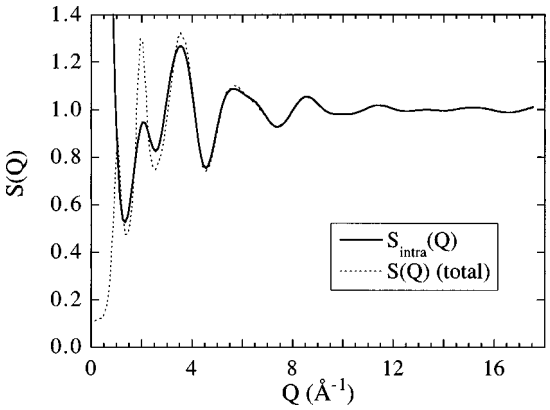

FIG. 9. Intramolecular contribution to the structure factor (solid line) and total structure factor (dotted line) derived from the simulation.

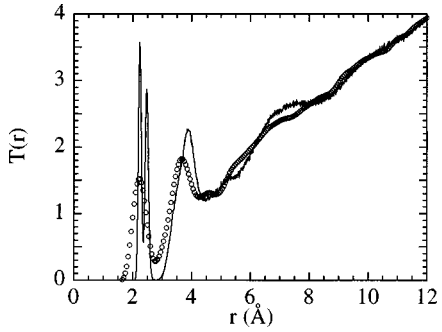

FIG. 10. Comparison of experimental pair-correlation function (circles) with that derived from the simulation described in Sec. IV (line).

liquid. Figure 10, which compares the total correlation function $T(r)$ from the simulation and from the experiment, reveals that the Fe-Cl intramolecular separation in the simulated molecules contains two peaks at 2.24 and 2.47 Å, corresponding to the terminal and bridging Cl atoms, respectively. However, the fit to the experimental peak in this region indicates a mean separation of 2.22 Å. The larger separations in the simulation cause shorter periodicity in $S_{\mathrm{FeCl}}(Q)$, the dominant contribution to $S(Q)$ above $Q=5$ Å, and lead to the discrepancies seen in Fig. 6. Figure 11 shows the partial pair-distribution functions $g_{ab}(r)=T_{ab}(r)/4\pi\rho r$, where the $T_{ab}(r)$ are derived from the $S_{ab}(Q)$ via Eq. (2), with intramolecular and intermolecular pairs identified separately. The similar first peak distances for intermolecular and intramolecular pairs in $g_{\mathrm{ClCl}}(r)$ results in both types of pairs contributing to the second peak in $S(Q)$. This distance is

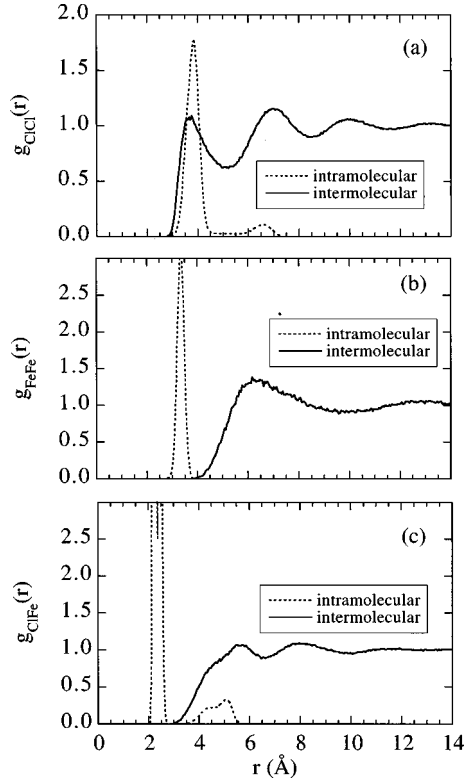

FIG. 11. Intra- and intermolecular contributions to the partial pair-distribution functions derived from the simulation.

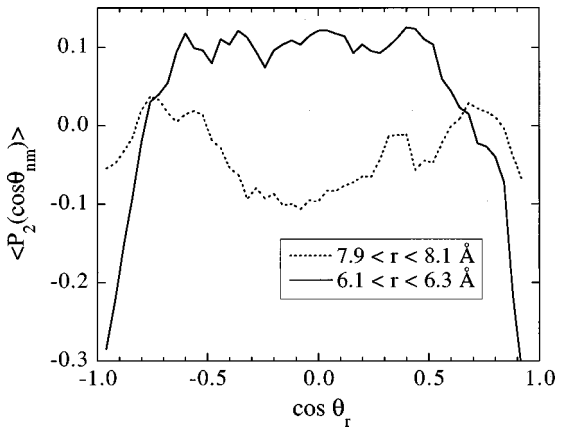

FIG. 12. Expectation value of the second Legendre polynomial of $\cos\theta_{nm}$ as a function of $\cos\theta_r$, derived from the simulation. $\cos\theta_{nm}=\mathbf{v}_n\cdot\mathbf{v}_m/|\mathbf{v}_n||\mathbf{v}_m|$ and $\theta_r=\cos^{-1}(\mathbf{r}\cdot\mathbf{v}_n/|\mathbf{r}||\mathbf{v}_n|)$, where $\mathbf{v}_n$ defines the orientation of molecule n and $\mathbf{r}$ is the vector joining the centers of molecules m and n.

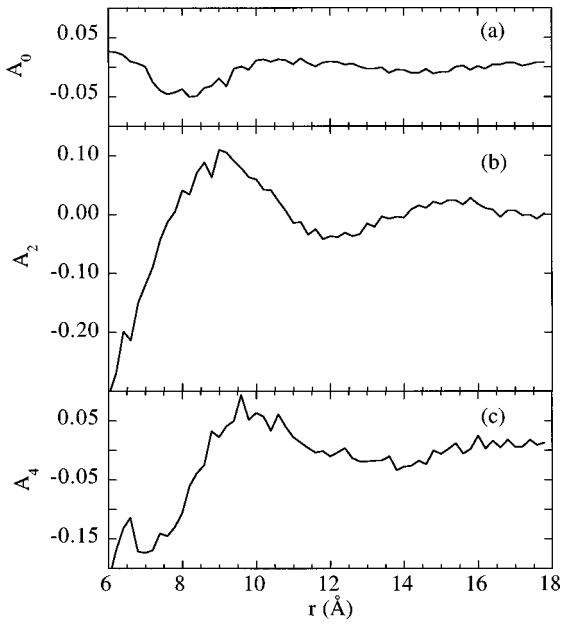

FIG. 13. First three even Legendre coefficients describing the distribution of $\cos\theta_{nm}$ in terms of $\cos\theta_r$, as a function of molecular separation r.

determined by bond lengths and angles for intramolecular pairs, while van der Waals interactions principally determine the separation for intermolecular pairs; the van der Waals radius of Cl in the simulation was 1.75 Å. The coordination number for Cl obtained from each peak is near 3, for a total of 6, in close agreement with the experimental result.

As mentioned above, the relative orientations of neighboring molecules play a key role in determining $S(Q)$, particularly at low Q. We have attempted to quantify such correlations following a procedure used earlier to analyze simulation results for an organic molecular liquid.[24] The orientation of a molecule is defined by a vector $\mathbf{v}$ extending from one Fe atom to the other. We calculate the expectation value for the second Legendre polynomial of the cosine of the angle made by the vectors of two neighboring molecules as a function of both the magnitude and direction of their separation (taken from the center of each molecule):

$$\langle P_2(\cos\theta_{nm})\rangle_{\mathbf{r}}=\frac{\sum_{n=1}^{N}\sum_{m}[(3\cos^2\theta_{nm}-1)/2]}{\sum_{n=1}^{N}\sum_{m}1}, \qquad (4)$$

where $\mathbf{r}$ is the vector joining the molecular centers, n sums over all of the molecules, m sums over the molecules separated from the nth molecule by $\mathbf{r}$, and $\cos\theta_{nm}=\mathbf{v}_n\cdot\mathbf{v}_m/|\mathbf{v}_n||\mathbf{v}_m|$. The separation direction is defined by the angle between $\mathbf{r}$ and the nth molecule's vector, $\theta_r=\cos^{-1}(\mathbf{r}\cdot\mathbf{v}_n/|\mathbf{r}||\mathbf{v}_n|)$. Figure 12 shows $\langle P_2(\cos\theta_{nm})\rangle$ versus $\cos\theta_r$ for two magnitudes of separation, $|\mathbf{r}|=6.2$ and 8.0 Å. As the figure illustrates, molecules to the side of other molecules ($\cos\theta_r\approx 0$) tend to align parallel at small separations, but at slightly larger separations the tendency switches to perpendicular alignment. To characterize the distance dependence of these curves more precisely we decompose them into Legendre polynomials:

$$\langle P_2(\cos\theta_{nm})\rangle_{\mathbf{r}}=\langle P_2(\cos\theta_{nm})\rangle_{r,\theta_r}=\sum_{0}^{\infty}A_l(r)P_l(\cos\theta_r), \qquad (5)$$

where the A_l are the Legendre coefficients

$$A_l(r)=\frac{2l+1}{2}\int_{-1}^{1}\langle P_2(\cos\theta_{nm})\rangle P_l(\cos\theta_r)d(\cos\theta_r). \qquad (6)$$

All coefficients with l odd are zero, reflecting the symmetry of the molecule. Figure 13 shows the coefficients for the first three even terms: A_0, A_2, and A_4. Except at the smallest separations A_0 is zero, indicating that molecules at a given separation *on average* have no preferred orientation. However, the changing sign of A_2 indicates that the direction-dependent orientational preferences oscillate between two types of behavior seen in Fig. 12 as the molecular separation increases.

A striking similarity exists between the orientational correlations described by Fig. 13 and those measured in a simulation of another molecular liquid, the organic glass former propylene glycol ($C_3O_2H_8$).[24] The formalism given above applies in this case also, with the vector $\mathbf{v}$ extending from one end C atom to the other. Figure 14 shows A_2 for $FeCl_3$ and propylene glycol with the distances normalized by the position of the first peak in the pair-distribution function for the molecular centers r_m for each liquid (see inset to Fig. 14.) The nearly identical orientational ordering in the two liquids, despite their distinct chemistry and molecular structure (propylene glycol has far lower molecular symmetry than iron chloride and is strongly hydrogen bonding), suggests that the ordering represented by these correlation functions is quite generic. In fact the two molecules have similar shapes: defining an aspect ratio $a=(L^3\rho/\eta)^{1/2}$, where ρ is

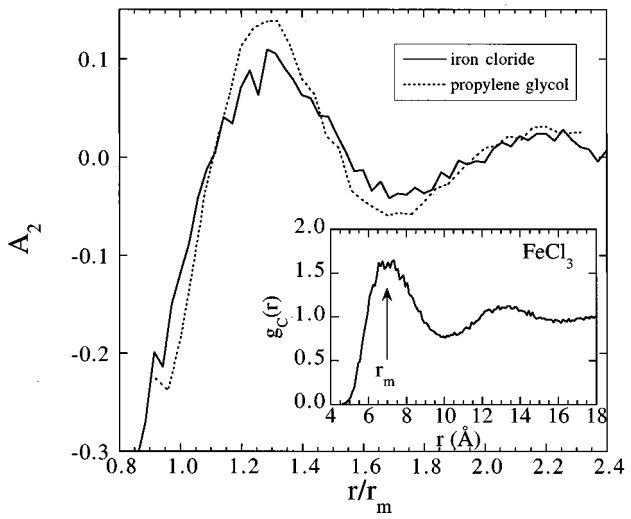

FIG. 14. Second even Legendre coefficients for molten $FeCl_3$ and liquid propylene glycol (Ref. 24), as a function of molecular separation r scaled with the value of r at the peak of the distribution function for the molecular centers (inset).

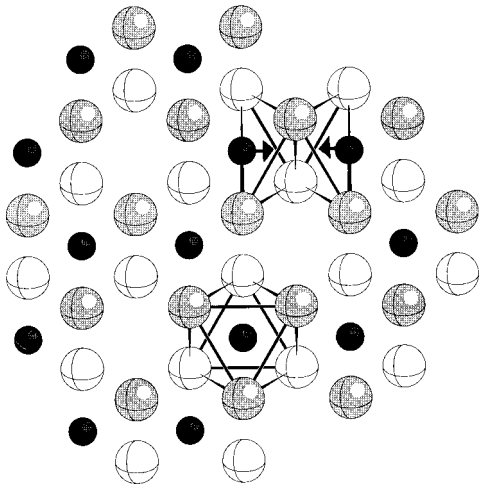

FIG. 15. Schematic illustration of melting in $FeCl_3$. The black spheres represent a plane of Fe ions in the crystal, and the gray and white spheres represent planes of Cl ions above and below the plane of Fe ions, respectively. The lower cluster represents the octahedral coordination of the Fe ions in the crystal, and the upper cluster the Fe_2Cl_6 molecule in the melt. The arrows indicate the required displacement of the two Fe ions upon melting.

the molecular number density, η is the packing fraction, and L is the length of the molecule in its longest direction, one obtains $a=1.01/\eta^{1/2}$ for iron chloride and $0.99/\eta^{1/2}$ for propylene glycol. However, a rigorous connection between molecular shape and the correlations in Fig. 14 has not been established.

V. CONCLUSIONS

The results of the present work show that melting in $FeCl_3$, associated with a large (63%) volume change, is accompanied by a change in local structure from the octahedral environment of the Fe in the solid to the tetrahedral environment of a Fe_2Cl_6 molecular liquid. A mechanism for such a transition, proposed by March and Tosi,[25] is shown in Fig. 15. Each Fe ion undergoes a substantial displacement, from an octahedral site between two triangles of Cl ions in adjacent planes, shown in the lower part of the figure, to a tetrahedral site between one Cl triangle and the Cl opposite it in the adjacent plane, as observed in the $AlBr_3$ crystal,[3] shown in the upper part of the figure. At the same time there must be a decrease in the packing of the Cl to account for the volume expansion. The reduced value for the second-neighbor coordination number observed in molten $FeCl_3$ is consistent with this reduction in Cl packing. Melting in $FeCl_3$ is clearly similar to that observed in $AlCl_3$ and in contrast to that of YCl_3 where an octahedral coordination is preserved on melting.[4]

The analysis of the bond distances and coordination numbers derived from the neutron-diffraction results shows that the short-range order of the liquid is very similar to that of Fe_2Cl_6 molecules in the vapor phase. However, in the liquid these molecules are strongly packed and spatially correlated with each other so that a given Cl ion will interact as strongly with its second-neighbor Cl ions on adjacent molecules as with those on the same molecule. This may explain the strong differences between the Raman spectra of the melt and vapor.[14–17]

A similar structure is obtained with a theoretical model of ionic interactions accounting for polarizabilities.[26] Recently, Akdeniz and Tosi[27] have suggested an ion transfer reaction

$$2\,Fe_2Cl_6 \rightarrow Fe_2Cl_5^+ + Fe_2Cl_7^- \qquad (7)$$

to explain the high conductivity of $FeCl_3$ compared with other molecular melts such has $AlCl_3$. This is consistent with the observation of a Raman peak associated with $Fe_2Cl_5^+$ in the melt. A fast exchange reaction of this type would reconcile the presence of strongly correlated Fe_2Cl_6 molecules deduced from the neutron-diffraction data with the difference between the Raman spectra of melt and vapor, which appears to be inconsistent with the presence of such molecules.

The modeling studies carried out in the present work show that the coupled orientational and positional ordering between the molecules can be reproduced satisfactorily using the $AlBr_3$ crystal structure as a starting point. The molecular-dynamics computer simulation shows that the molecules tend to align parallel at small separations and perpendicular at larger separations. Comparison with the organic molecular liquid propylene glycol suggests that this ordering occurs quite generally.

ACKNOWLEDGMENTS

We are grateful to K. J. Volin and the Operations Staff of the Intense Pulsed Neutron Source for experimental assistance and to L. A. Curtiss, M. P. Tosi, Z. Akdeniz, and S. R. Nagel for helpful discussions. This work was performed under the auspices of the U.S. Department of Energy, Division of Materials Sciences, Office of Basic Energy Sciences, under Contract No. W-31-109-ENG at Argonne National Laboratory, Grant No. DE-FG05-87ER-45325 at the University of Houston and Grant No. DE-FG02-92ER-25119 at the University of Chicago.

[1] M. P. Tosi, D. L. Price, and M.-L. Saboungi, Annu. Rev. Phys. Chem. **44**, 173 (1973).
[2] R. W. G. Wyckoff, *Crystal Structures* (Wiley Interscience, New York, 1964), Vol. 2, Chap. VB.
[3] P. A. Renes and C. H. MacGillavry, Recl. Trav. Chim. Pays-Bas. **64**, 275 (1945).
[4] M.-L. Saboungi, D. L. Price, C. Scamehorn, and M. P. Tosi, Europhys. Lett. **15**, 283 (1991).
[5] M. P. Tosi, G. Pastore, M.-L. Saboungi, and D. L. Price, Phys. Scr. **T39**, 367 (1991).
[6] M.-L. Saboungi, M. A. Howe, and D. L. Price, Mol. Phys. **79**, 847 (1993).
[7] Y. S. Badyal, D. A. Allen, and R. A. Howe, J. Phys.: Condens. Matter **6**, 10 193 (1994).
[8] D. L. Price, M.-L. Saboungi, S. Hashimoto, and S. C. Moss, in *Proceedings of the 8th International Symposium on Molten Salts*, edited by R. J. Gale, G. Blomgren, and H. Kojima (Electrochemical Society, Pennington, NJ, 1993), p. 14.
[9] E. Z. Zasorin, N. G. Rambidi, and P. A. Akishin, Zh. Strukt. Khim. SSSR **4**, 910 (1963) [J. Struct. Chem. **4**, 836 (1963)]; M. Hargettai, J. Trummell, and J. Hargettai, J. Chem. Soc. Dalton Trans. **1**, 87 (1980).
[10] Y. S. Badyal, M.-L. Saboungi, D. L. Price, D. R. Haeffner, and S. D. Shastri, Europhys. Lett. **39**, 19 (1997).
[11] K. Forster, S. Hashimoto, and S. C. Moss, in *Proceedings of the Symposium on Graphite Intercalation Compounds: Science and Applications*, edited by N. Endo, M. S. Dresselhaus, and G. Dresselhaus (Materials Research Society, Pittsburgh, 1988), p. 25.
[12] S. Hashimoto, K. Forster, and S. C. Moss, Acta Crystallogr., Sect. A: Found. Crystallogr. **44**, 897 (1988).
[13] S. Hashimoto, K. Forster, and S. C. Moss, J. Appl. Crystallogr. **22**, 173 (1989).
[14] M. H. Brooker and G. N. Papatheodorou, in *Advances in Molten Salt Chemistry*, edited by G. Mamantov (Elsevier, Amsterdam, 1983), Vol. 5.
[15] G. A. Voyiatzis (unpublished).
[16] C. Cramer and M. Grimsditch (private communication).
[17] L. Nalbandian and G. N. Papatheodorou, High. Temp. Sci. **28**, 49 (1990).
[18] G. Scholtz and L. A. Curtiss (unpublished).
[19] E. J. Lisher and J. B. Forsyth, Acta Crystallogr., Sect. A: Cryst. Phys., Diffr., Theor. Gen. Crystallogr. **27**, 545 (1971).
[20] D. L. Price, S. C. Moss, R. Reijers, M.-L. Saboungi, and S. Susman, J. Phys.: Condens. Matter **1**, 1005 (1989).
[21] P. A. Egelstaff, D. I. Page, and J. G. Powles, Mol. Phys. **20**, 881 (1971).
[22] S. C. Moss and D. L. Price, in *Physics of Disordered Materials*, edited by D. Adler, H. Fritzsche, and S. R. Ovshinsky (Plenum, New York, 1985), p. 77.
[23] Discover User Guide, version 2.9.5 and 94.0, Biosym Technologies, San Diego, 1994.
[24] R. L. Leheny, N. Menon, S. R. Nagel, D. L. Price, K. Suzuya, and P. Thiyagarajan, Chem. Phys. **105**, 7783 (1996).
[25] N. H. March and M. P. Tosi, Phys. Chem. Liquids **10**, 39 (1980).
[26] Z. Akdeniz, G. Pastore, and M. P. Tosi, Phys. Chem. Liq. (to be published).
[27] Z. Akdeniz and M. P. Tosi (unpublished).